In-situ interaction between different concretes and Opalinus Clay

A. Jenni[a*], U. Mäder[a], C. Lerouge[b], S. Gaboreau[b], B. Schwyn[c]

[a] RWI, Institute of Geological Sciences, University of Bern, Baltzerstrasse 3, CH-3012 Bern, Switzerland (andreas.jenni@geo.unibe.ch, urs.maeder@geo.unibe.ch), +41 31 631 4531

[b] BRGM, F-45060 Orléans Cedex 2, France, (c.lerouge@brgm.fr, s.gaboreau@brgm.fr)

[c] Nagra, CH-5430 Wettingen, Switzerland (bernhard.schwyn@nagra.ch)

[*] corresponding author

Abstract

Interactions between cementitious materials and claystone are driven by chemical gradients in pore water and might lead to mineralogical modifications in both materials. In the context of a radioactive waste repository, this alteration might influence safety-relevant clay properties like swelling pressure, permeability, or specific retention. In this study, interfaces of Opalinus Clay, a potential host-rock in Switzerland, and three concrete formulations emplaced in the Cement-Clay Interaction (CI) Experiment at the Mont Terri Underground Laboratory (St. Ursanne, Switzerland) were analysed after 2.2 years of interaction.

Sampling techniques with interface stabilisation followed by inclined intersection drilling were developed. Element distribution maps of the concrete-clay interfaces show complex zonations like sulphur enrichment, zones depleted in Ca but enriched in Mg, strong Mg enrichment adjacent to the interface, or carbonation. Consistently, the carbonated zone shows a reduced porosity. Properties of the complex zonation strongly depend on cement properties like water content and pH (ordinary Portland cement vs. low-pH cement).

An increased Ca or Mg content in the first 100 µm next to the interface is observed in Opalinus Clay. The cation occupancy of clay exchanger phases next to the ordinary Portland cement interface is depleted in Mg, but enriched in Na, whereas porosity shows no changes at all.

The current data suggests migration of CO_2/HCO_3^-, SO_4^{2-}, and Mg species from clay into cement. pH decrease in the cement next to the interface leads to instability of ettringite, and the sulphate liberated diffuses towards higher pH regions (away from the interface), where additional ettringite can form.

Keywords

cement-clay interaction, diffusion, low pH cement, near field, drilling technique, Mont Terri

Highlights

- Interfaces between Opalinus Clay and three types of concrete (ordinary Portland cement, low pH slag cement, low pH shotcrete) were investigated by SEM EDX and other methods.
- Strong gradients in pore water chemistry between cements and clay drive ion diffusion leading to the observed chemical and mineralogical zonations.
- Carbonation coincides with porosity reduction in cement.

1. Introduction

Designs for geological disposal of radioactive waste foresee cementitious materials as structural elements, backfill or waste matrix. Interactions take place at interfaces of contrasting materials driven by chemical gradients in pore water causing diffusive fluxes of dissolved species. This may lead to mineralogical alterations in the barrier system, which in turn are expected to locally influence properties like permeability, swelling pressure or specific retention properties in the case of concrete in contact with claystone or compacted bentonite. Laboratory experiments (Adler, 2001; Adler et al., 2001; Dauzères, 2010; Dauzères et al., 2010) and in-situ experiments (Gaboreau et al., 2011; Read et al., 2001; Tinseau et al., 2006) demonstrate alteration of both cement and claystone adjacent to interfaces. An increase in porosity in the cement close to the interface, and clogging in the claystone adjacent to it are commonly predicted by reactive transport modelling (De Windt et al., 2008; Kosakowski and Berner, 2013; Marty et al., 2009). Changes in porosity distribution - and therefore also permeability - near such interfaces is an important process governing the long-term physicochemical evolution of the engineered barrier and its geological near-field (Kosakowski and Berner, 2013). Clay-rich rocks currently under consideration at an advanced stage of repository planning include Opalinus Clay (OPA) in Switzerland (Nagra, 2002), Callovo-Oxfordian "argillite" in France (ANDRA, 2005), and Boom Clay in Belgium (SCK•CEN, 2012). Clay-based engineered barrier materials include compacted bentonite and sand/bentonite mixtures, among others.

The Cement-Clay Interaction (CI) Experiment carried out at the Mont Terri underground research laboratory is aimed at reducing uncertainties in process understanding related to cement-clay interfaces by providing a detailed analysis of mineralogical changes over relatively long time periods and under realistic boundary conditions. This contribution is a first account in the open literature of this effort covering the first 2.2 years since implementing a field experiment in the rock laboratory. Central to this effort was also the development of an excavation technique to recover physically undisturbed samples of interfaces, and optimise a number of analytical tools. The interpretation is based purely on the analytical data and existing system understanding, but will be augmented by reactive transport modelling in the near future. Several meeting abstracts have been published covering some aspects of the CI Experiment (Jenni et al., 2012, 2013). Companion studies address cement hydration of reference samples (Lothenbach et al., 2012; Lothenbach et al., 2014; Lothenbach and Wieland, 2006), and develop new high-resolution techniques for phase identification using µ-X-ray diffraction at the Paul Scherrer Institut (Dähn et al., 2014).

2. Setup, materials, and drilling technique for sampling

A duration of at least 20 years is foreseen for the CI Experiment at the Mont Terri Underground Laboratory (St. Ursanne, Switzerland, www.mont-terri.ch). The field experiment comprises two vertical boreholes (386 mm diameter, up to 9 m length) in OPA, filled each with sections of three different concretes and also a section of compacted bentonite (Fig. 1). The experiment is located in the HE-D niche adjacent to Gallery-98 which was excavated in 1998. The floor of the gallery and niche is a thick concrete plate (40-60 cm) and the walls are protected by shotcrete. The extent of the excavation disturbed zone is known to increase with time and may reach several meters depending on orientations of bedding and gallery, and in this region moderate suction may be observed (undersaturated hydrologic conditions). Two monitoring boreholes record pore water pressure in OPA. Locations of inclined boreholes used for two sampling campaigns are shown schematically. The large-diameter vertical boreholes were air-drilled with triple-barrel coring equipment during March/April 2007. The boreholes were immediately argon filled and kept closed until emplacement of the different concretes and bentonite during April 2007. The borehole walls were brushed and vacuum cleaned to avoid any dust, and the walls were also protected during emplacement of the different concrete mixtures. Each concrete mixture was prepared in 40 L batches, cast into the boreholes and vibrated. The concrete work was accompanied by standard quality control tests. Bentonite was emplaced as a mixture of highly compacted pellets and fines, and a concrete lid with a water saturation system was placed on top, and sealed against the overlying concrete section.

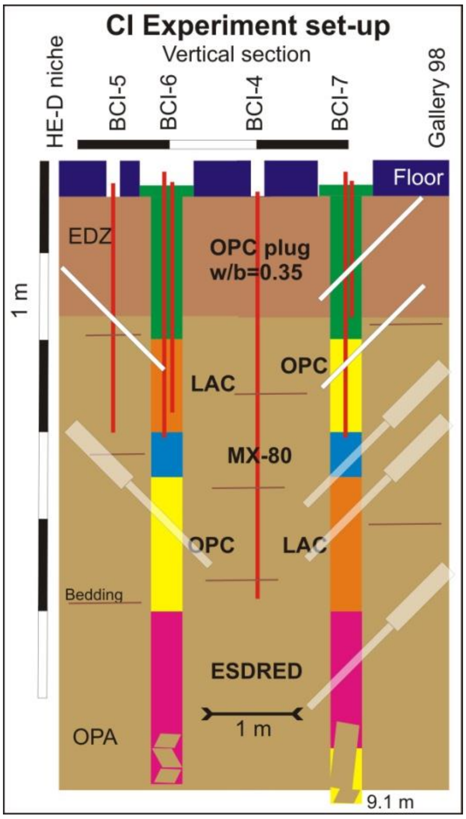

Fig. 1 Setup of the CI Experiment drawn to scale with distribution of concrete sections and bentonite in two vertical piles, and monitoring boreholes (dark grey). Sampling boreholes inclined at 45° are shown for the 2009 sampling campaign (white) and the 2012 campaign (telescoped). Sampling was drilled at 90° to the section shown. EDZ: excavation-disturbed zone of the gallery; OPA: Opalinus Clay; OPC: ordinary Portland cement; LAC, ESDRED: low-pH cement; MX-80: bentonite section.

Preserved core sections of OPA (284 mm outer diameter) from drilling the vertical boreholes were cut square to ca. 40 cm length by a large mechanical saw and vacuum packed for interim storage. Nine such sections were encased in the same three different concretes in 120 litre plastic drums. These drums serve as “dummy experiments” containing the same type of interfaces, but being more readily available for sampling and any desired technical or analytical tests.

Monitoring equipment includes two packed-off small-volume borehole intervals in OPA (Fig. 1) for monitoring pore water pressures, total pressure (swelling pressure) and pore water pressure sensors in the bentonite sections, temperature sensors (integrated in pressure sensors), and pressure sensors in two packed-off intervals in the concrete sections above the bentonite sections (shown as vertical lines within BCI-6 and BCI-7). Liquid pressures are measured above ground connected to the test section by polyamide lines, solid pressure sensors for swelling pressures were encased in the concrete lids and face the bentonite section, with membranes of 20 mm diameter. Monitoring serves (1) to confirm pore water pressures above ambient or detect suction, (2) to monitor swelling (saturation progress) of the bentonite sections, and (3) to allow for sampling of pore water in the concrete sections (though this has not been done to date).

2.1. Opalinus Clay

OPA was identified and selected as a host-rock for the final disposal of radioactive waste in Switzerland (Nagra, 2002). The approximately 170 million year old marine claystone formation is described in a comprehensive report (Pearson et al., 2003). The CI Experiment is located in the shaly facies, which consists of approximately 62 wt% clay minerals (24 wt% kaolinite, 20 wt% illite, 10 wt% illite/smectite mixed layers, 8 wt% chlorite), 3 wt% feldspars, 20 wt% calcite, 2 wt% siderite, 1 wt% dolomite/ankerite, 10 wt% quartz, 1 wt% pyrite, <1 wt% organic carbon. The average total porosity is ~16%, and the average pore water composition is given in Table 1.

2.2. Concretes

The concrete formulations are based on common aggregate content and grain size distributions (sand and gravel up to 16 mm), combined with three different cements: Portland cement (OPC), ESDRED shotcrete cement especially designed for repository applications (40% of cement substituted with silica fume), and a low alkali cement (LAC, containing slag and nanosilica). Both silica fume and nanosilica consist of mainly amorphous silica with approximately 100 nm and 12 nm average grain diameter, respectively. Further details on the materials are provided in Table 2 and Table 3 (Lothenbach et al., 2012; Lothenbach et al., 2014; Lothenbach and Wieland, 2006). Material suppliers are Holcim Switzerland (CEM I 42.5 R HS “Protego 4R”, CEM I 42.5 N “Normo 4”), Jura Cement Switzerland (CEM III/B 42.5 L “JURANIT”), Sika Switzerland (silica fume “SikaFume HR/TU”, accelerator “Sigunit L53 AF”), Degussa Switzerland (nanosilica “Aerosil 200”, superplasticiser “Glenium C321”), TFB Switzerland (sand and gravel, according to SN EN 12620, rounded river sediment).

Pore water	Age [days]	**Ca** [mmol/l]	**Mg** [mmol/l]	**Na** [mmol/l]	**K** [mmol/l]	**S** [mmol/l]	**Cl** [mmol/l]	**C** [mmol/l]	**pH**
OPC		24 - 2.9	<	26 - 90	137 - 209	66 - 4.5	<		13 - 13.3
LAC	0.04 - 1310	20 - 2.7	0.0018 - 0.0011	18 - 23	26 - 17	25 - 22	<	~0.05	12.4 - 12.2
ESDRED		25 - 29	0.0063 - 0.0045	79 - 22	186 - 11	45 - 1.8	<		12.4 - 11.7
gradient		↑	↑	↑	↓	↑	↑	↑	↓
Opalinus		25	19	225	5	30	256	~4	7

Table 1 Comparison between pore water chemistries of cements at different ages and Opalinus Clay (Bradbury and Baeyens, 1998; Lothenbach et al., 2012; Lothenbach et al., 2014; Lothenbach and Wieland, 2006). Arrows indicate direction of chemical gradients, or OH^- gradient in case of pH.

		OPC	**ESDRED**	**LAC**
CEM I 42.5 R HS	[kg/m^3]	490	-	-
CEM I 42.5 N	[kg/m^3]	-	210	-
CEM III/B 42.5 L	[kg/m^3]	-	-	206
silica fume	[kg/m^3]	-	140	-
nanosilica	[kg/m^3]	-	-	22.9
superplasticiser	[kg/m^3]	3.0	4.2	6.0
accelerator	[kg/m^3]	-	16.8	-
water	[kg/m^3]	172	175	247
water/binder weight ratio	-	0.35	0.50	1.08
sand, gravel	[kg/m^3]	1904	1800	1704
Cement composition:				
alite	[wt%]	52.7	52.8	16.7
belite	[wt%]	14.4	22.8	5.6
aluminate	[wt%]	1.1	5.0	0.6
ferrite	[wt%]	17.2	7.9	3.4
periclase	[wt%]	3.3	1.0	0.3
calcite	[wt%]	1.7	2.9	3.9
quartz	[wt%]	0	0.5	0.3
anhydrite	[wt%]	1.0	1.9	0
hemihydrite	[wt%]	2.2	1.7	0
gypsum	[wt%]	3.8	0	2.2
syngenite	[wt%]	0	2.0	0
dolomite	[wt%]	2.5	1.5	0.7
amorphous	[wt%]	-	-	65.9

Table 2 Characteristics of concretes and cements. Binder represents all reactive components (cement, slag, silica). Cement compositions and amorphous contents were determined by XRD Riedtveld analysis using an internal standard.

	[g/100g]
CaO	38.0
SiO_2	37.0
Al_2O_3	13.0
Fe_2O_3	0.1
MgO	7.6
Na_2O	0.2
K_2O	0.3
SO_3	3.2

Table 3 Slag composition in CEM III/B 42.5 L (65.9% slag), calculated from XRF measurement of total cement and mineralogy shown in Table 2.

The hydration of OPC, ESDRED, and LAC is described in detail elsewhere (Lothenbach et al., 2012; Lothenbach et al., 2014; Lothenbach and Wieland, 2006). While portlandite is abundant and pH is still high in OPC after 3.5 years, both ESDRED and LAC lack portlandite and show lower pH values. Also, Ca/Si ratios in calcium silicate hydrate (CSH) of the latter concretes are significantly lower, which favours the uptake of Al and alkalis. Original OPC and LAC mixtures are exceptionally high in Mg. XRD and TGA measurements indicate the presence of hydrotalcite as Mg-phase. Nanosilica in LAC has completely reacted, whereas unreacted slag (approximately 20% of original slag in LAC) and unreacted silica fume (almost 50% of original content in ESDRED) is still observed after 3.5 years of hydration.

All three cements generate significantly different pore fluid chemistries from first water contact onwards, and the compositions change during hydration (overview in Table 1). The enormous chemical gradients towards the OPA pore water, mainly in pH, dissolved carbon, and Mg, are considered driving forces for chemical interaction.

2.3. Sampling

The sampling strategy foresees repeat inclined intersection drilling to recover interface samples at desired time intervals (Fig. 1). A first drilling campaign was carried out after 2.2 years (May and July, 2009) with simple drilling equipment to reach maximum borehole depths of 3-4 m. The interfaces were stabilised by a small central pilot hole in which a reinforcement rod of either threaded steel or an aluminium tube was cemented in (Fig. 2). This reinforced section was overcored with a single-barrel 86 mm OD tool equipped with a core catcher using a simple Hilti drill and compressed air. This operation was only partially successful, and the interfaces separated slightly due to mechanical forces during overcoring and extraction. Nevertheless, the exact contact between clay and concrete was preserved for two of the three types of concrete, while ESDRED concrete was located too deep to be reached by this low-cost operation. A drum sample (see above) was used instead, cored with the same drilling equipment. All sampling boreholes from this first campaign were filled with cement slurry of the same type as sampled. OPC type concrete was sampled in the sealing plug (Fig. 1) that had a much lower water/binder ratio compared to the OPC concrete emplaced in the proper test sections below. Concrete-bentonite interfaces were not sampled at that time.

A second sampling campaign was carried out in February 2012 with adequate drilling equipment to reach depths to 12 m with state-of-the art triple barrel drilling equipment for overcoring. A new and improved technique for stabilising all interfaces was designed. The drilling procedure (Fig. 2) included: (1) drilling of an approach borehole with 200 mm diameter to a distance of 40-50 cm from the interface; (2) reaming the base square to the borehole axis; (3) inserting a drilling template for 6 boreholes with 46 mm diameter arranged on a circle around the centre; (4) drilling of 3 out of the 6 small boreholes to penetrate both the interface at the front of the vertical pile as well as that located at the back; (5) inserting fibreglass anchors of 36 mm diameter with a setting tool and injecting epoxy resin to glue them in (anchor tubes were pre-filled with mortar for mass and later drillability, and contain a resin injection line for bottom-up injection); (6) drilling of remaining 3 small boreholes, and inserting anchors as indicated before; (7) removal of anchor setting tools and resin injection lines; (8) overcoring of the reinforced section with a triple-barrel tool with 156 mm outer diameter to 20-40 cm below the reinforcements for core catching in the pristine claystone. This procedure yielded compound cores of 10.1 cm diameter and up to 140 cm length containing at least two physically intact interfaces, with parts of the 6 reinforcements laminating the core along the outer surface. Drilling of the small anchor boreholes through saturated bentonite sections required special attention because this material cannot be abraded by diamond drilling tools. Instead, thin-walled drilling rods without crown were simply pushed 20-30 cm into bentonite at a time and then cores were pulled with a slow rotation. This yielded clean anchor boreholes, but the corresponding small bentonite cores were elongated according to the volume displaced by the cross section of the drilling tube. The actual bentonite core sections were recovered undeformed, because drilling was done mainly through the mortar-filled anchors with only little bentonite in-between. In one case it was possible to sample 3 interfaces in a single core: two vertical interfaces between concrete and bentonite against claystone, and a horizontally oriented interface between concrete and bentonite. Materials sampled with the new and improved technique are presently under investigation.

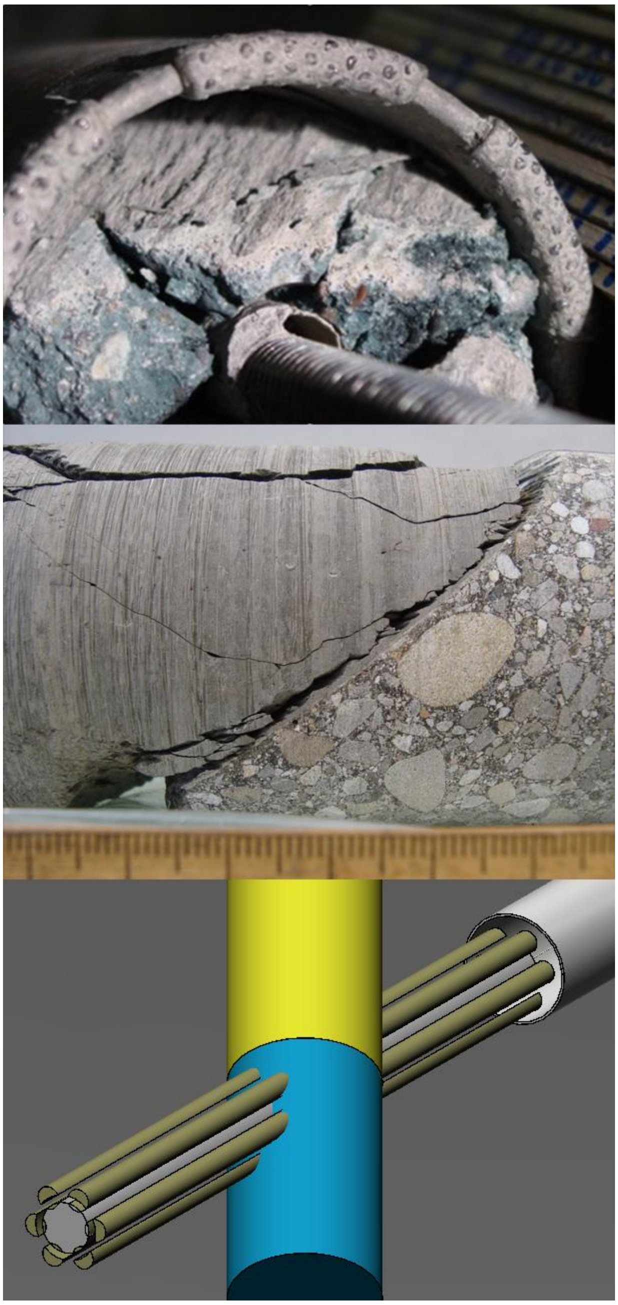

Fig. 2 Example of drilling technique used in 2009 with a single re-enforcement glued in prior to overcoring (upper images, outer diameter of drillbit = 86 mm). Shown is a sample of LAC with white reaction zone at interface, and a thin layer of Opalinus Clay preserved at the interface (top), and OPC (sealing plug) mechanically separated from Opalinus Clay (middle). Schematic of optimised stabilisation technique used in 2012 (lower image, see text for explanation).

3. Methods

A detailed analysis of concrete/OPA interfaces after a certain interaction time reveals fingerprints of the mechanisms active during this time interval. Several mechanisms are superimposed and produce in each type of concrete-OPA interface 3-6 interaction zones with distinct compositional characteristics. This leads to an overwhelming quantity of observations, multiplied by the number of sampling intervals. In this study, we concentrate on the first sampling interval of 2.2 years. Our analysis is restricted to the cement matrix in-between the aggregates, and the clay matrix. In this context, only methods with a spatial resolution of less than 30 µm can analyse the interaction layers with thicknesses down to similar values. Furthermore, these layers are parallel to a microscopically irregular interface. All analyses avoid sampling of sand and multi-mineral aggregate in the concrete, or pyrite nests, bioclasts, and sand layers in OPA. The application of bulk methods is therefore in most cases unsuccessful.

3.1. Microscopy

Polished sections and thin sections across the concrete-OPA interface were prepared without water contact. Exposure to water, or to high air humidity for a prolonged time interval, may rehydrate remaining clinker phases in the cement, dissolve cement hydrates, or lead to swelling of clay minerals in OPA. Large differences in hardness and the mechanically weak interfaces pose additional challenges for sample cutting and handling. The samples were first embedded in resin, then the surface to be analysed was chosen at 45° to the interface plane, and cutting was done with a diamond saw using petroleum as lubricant. The cut surface was processed using grinding paper, oil-based diamond suspensions and petroleum, resulting in good quality thin sections for light microscopy, or polished sections for the scanning electron microscope.

The uncoated sample surface was examined in a SEM (Zeiss EVO-50 XVP) equipped with a EDAX Sapphire light element detector in the low vacuum mode (10 Pa) with a beam acceleration of 20 kV and a working distance of 8.6 mm. The beam current was adjusted to yield a dead time of 20-30% for EDX analysis (energy dispersive spectroscopy). EDX element maps with a resolution of 512x400 pixels were acquired using a dwell time of 200 µs, and frames were averaged for 8-12 h. Higher resolution (1024x800 pixels), but lower dwell time was used to acquire backscatter electron (BE) images, which depict the average proton number at beam location. Brightness and contrast of the maps were adjusted to reveal gradients within cement or clay matrix, often resulting in over- or undersaturation of phases of no interest. EDX point measurements were acquired for 60 s live time and semi-quantitatively analysed without standardisation using the EDAX Genesis software (ZAF matrix correction). All detected elements heavier than fluorine are normalised to 100 wt%, in contrast to methods with standards resulting in absolute compositions (e.g., microprobe). Errors are below 2 wt% in low-vacuum mode. The skirt effect broadens the beam in low vacuum and leads to an increased measurement volume. However, all measurements in the cement matrix are treated as measurements of phase mixtures, because the grain size of hydrates is expected to be below the measurement volume of approximately 1-2 µm in diameter.

Transmission and reflective light micrographs were acquired using a Zeiss EVO-50 XVP microscope equipped with a CCD camera.

3.2. Raman spectroscopy

Raman spectroscopy was performed with a Jobin Yvon LabRAM-HR800 instrument, consisting of an Olympus BX41 confocal microscope coupled to an 800 mm focal-length spectrograph. A He-Ne laser (20 mW, polarised 500:1) with an excitation wavelength of 632.817 nm (red) was focused on the sample surface and the Raman signal was collected in backscattered mode. The sampled volume was a few µm^3 using a 100x objective. Acquisition time for pyrite/ hematite was 2x10 s, and 2x120 s were used for clay or cement matrices. The spectra were recorded with Labspec V4.14 software. Fluorescence caused an enormous background in cement and clay matrices, which only allowed for reliable identification of calcite. The fluorescence is blamed on the organic additives added to the cements, and on natural organic matter present in OPA.

3.3. Porosity characterisation

Autoradiography was performed according to the method developed for clay materials (Pret et al., 2004). Selected sections were oven dried during 5 days at 75°C under vacuum. The conditions used for the cement materials were chosen according to the work of Galle (Galle, 2001), which showed the impact of drying cement materials. The samples were impregnated over 40 days with ^{14}C MethylMethAcrylate (MMA) with a tracer activity of 6.0 µCi/mL. The objective was to reach a total saturation of the pore space by the resin (including interlayer space) in order to obtain quantitative porosity measurements by autoradiography. The polymerisation of the impregnated samples was triggered by ^{60}Co irradiation with a total dose of 71 kGy (Pret et al., 2004). The textural state of the impregnated samples can be expected to be close to the textural state encountered for samples in equilibrium with a water activity of 0.98 (Pret et al., 2010). This was mainly a result of the properties of the resin (viscosity and dipole moment), which are close to those of water. Two polished sections were prepared with a low speed diamond saw cutting impregnated samples in half. Samples were then polished using diamond powders with grain sizes down to 1 µm.

Kodak Biomax MR film was then exposed to the thick sections for 9 days. Exposure times were optimised according to different porosities of claystone and cement materials to acquire the best porosity contrast (Pret et al., 2004). The autoradiographs were then digitised with 8 bit greyscale and a resolution of 2400 dpi (10.4 µm pixel size). The local blackening of the film (expressed by a local optical density) is proportional to the local concentration of radioactive resin. Sets of calibration sources of known activity were simultaneously exposed on the autoradiograph film to obtain the relationship between the local activities and optical densities by fitting the experimental data using a well-known calibration function (Hellmuth et al., 1993). With the calibration function and the tracer activity, a local mean porosity was then calculated with autoradio software (Pret et al., 2004) for each pixel of the digitised autoradiographs using the relationships documented elsewhere (Sammartino et al., 2002). Such a local pixel-size porosity includes the connected micro-, meso-, and macro-porosity. For each autoradiograph, a combination of analysis methods was applied to reveal a porosity distribution. Porosity frequency histograms were computed on different sub-areas of the autoradiographs by counting the number of pixels with similar porosity values. Porosity maps were then computed to localise spatial heterogeneities, by displaying the local porosity of each pixel using a linear grey scale ranging between two selected porosity values identified on the histogram.

3.4. Selective micro-sampling: infrared spectrometry, aqueous leaching, sulphur content, and cation exchange capacity

The concrete and the clay stone parts of the samples were separated, glued on two separate glass thin sections, and the matrices were sampled with a micro-drill starting at the interface, progressing away from it. Concrete aggregates, sand grains, bioclasts, or pyrite were avoided as much as possible. Sampling intervals were close near the concrete/clay interface (1 mm, then 2 mm) and more spaced further from it (5 mm, then 10 mm). Each sample, consisting of a fine-grained powder, was weighed. 1 mg was used for infrared (IR) spectrometry measurements. The remaining powder was dedicated to leaching and cation exchange measurements.

IR spectrometry was performed on bulk powders of both concrete and claystone samples to identify dissolution, precipitation, and to define the crystalline state of phases. IR spectra were obtained on a BRUKER Equinox IFS55 spectrometer by transmission through a pellet made of a mixture of 250 mg KBr with 1 mg of sample. 32 scans were performed for each spectrum from 4000 to 350 cm^{-1}. The spectral resolution for this study was always 4 cm^{-1}.

Aqueous leaching was performed on both concrete and claystone samples. Bulk powders were leached with deionised water that was boiled and degassed under N_2. For each sample, a leaching test was performed on 100 mg of powder. The water/rock ratio was 10, and the time of leaching was 30 minutes. After the leaching procedure, the liquid was centrifuged at 4500 rpm for 10 min and passed through a 0.1 μm filter prior to analysis. Sulphate concentrations were measured by ion chromatography, with a detection limit of 0.1 mg/l.

The residual solid of concrete after aqueous leaching was dried and analysed for sulphur content using a Horiba (Jobin Yvon Emia-320V) C/S Elemental Analyser. Samples were heated at 850°C under oxygen flux. The produced CO_2 and SO_2 were measured by IR spectrometry.

Cation exchange capacities (CEC) and cation selectivities were measured on bulk powders of claystone samples. CEC was measured by exchange of 100 mg of powder with cobalt hexamine trichloride over 30 minutes at room temperature with a reagent/solid mass ratio of 20 (Ciesielski and Sterckeman, 1997; Rémy and Orsini, 1976). The suspension was centrifuged and the supernatant filtered. Major cation (Na^+, K^+, Ca^{2+}, Mg^{2+}) concentrations in the supernatant solution were determined by ion chromatography (KOH eluent, KOH suppressor at column exit), with a DIONEX conductivity detector (detection limit of 0.5 mg/l). The total CEC was obtained from the cobalt hexamine concentration in the leachate determined by colorimetry (absorption band at 473 nm) on a UNICAM UV visible spectrometer. The good agreement between the sum of measured cations and the total CEC obtained from cobalt hexamine colorimetry indicates a negligible contribution of cations from dissolved phases.

4. Results and discussion

4.1. Chemical zonations parallel to the interface

SEM BE images, EDX maps, and light microscopy (Fig. 3 and Fig. 4) show distinct zones in the cement matrix parallel to the concrete-clay interface. The exact geometry of these zones can be influenced by concrete aggregates or cracks. Depending on the cement properties, up to 6 chemically distinct zones can be discriminated with a total thickness of approximately 2-4 mm. The zones were numbered starting from the contact; zones with the same number from different cements do not correspond to each other. Only one distinct zone was observed in the claystone close to the interface with OPC and LAC. All subsequent descriptions of Fig. 3 and Fig. 4 refer to the cement or OPA matrix only; aggregates, sand grains, calcite bioclasts, pyrite, or other inclusions are neglected.

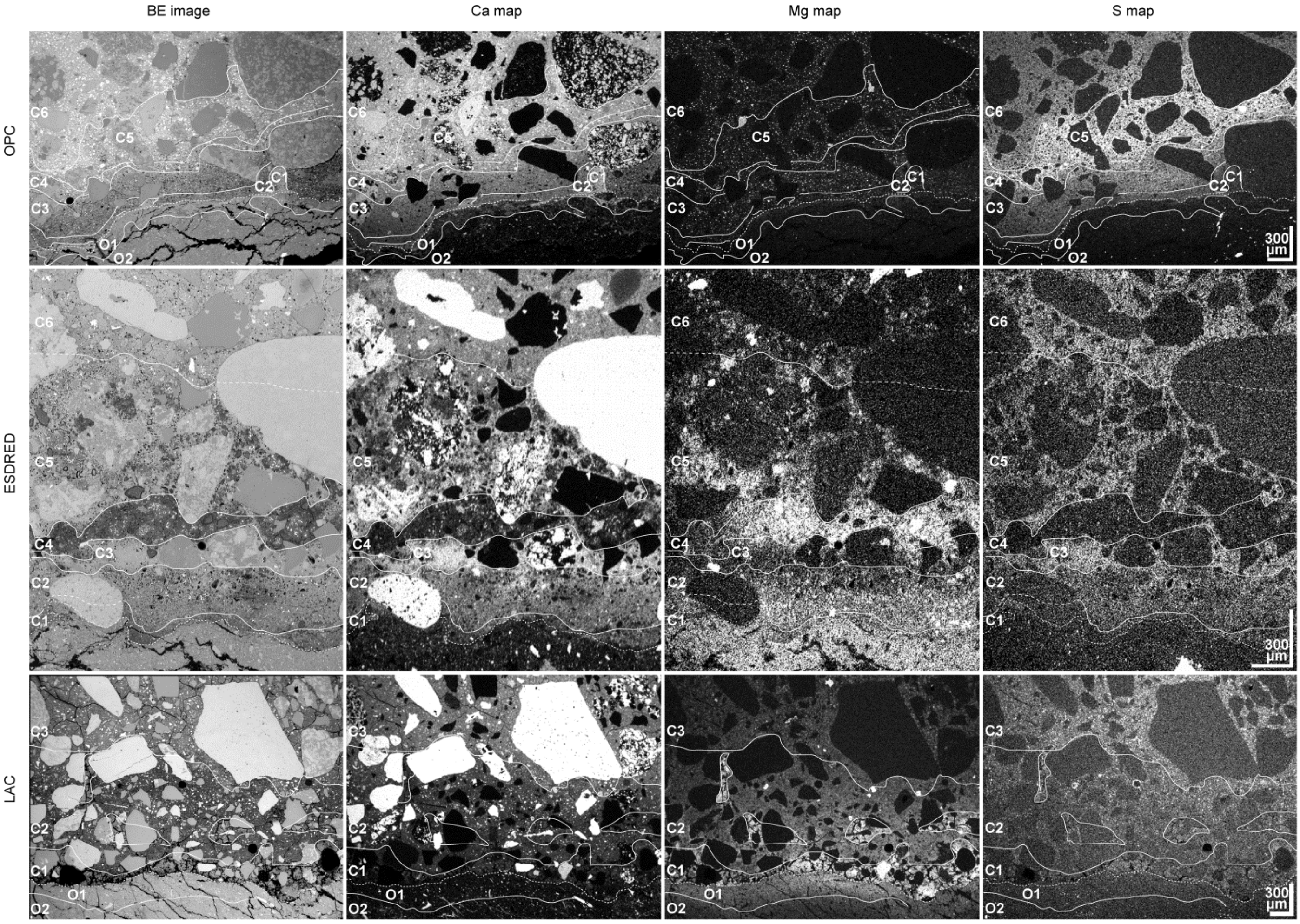

Fig. 3 SEM BE images and Ca, Mg, and S EDX maps of sections across the OPA-cement interface. The vertical scale (distance from the interface) is calculated from the angle between image plane and interface plane (ca. 45°) and it is indicated as a vertical scale bar. The horizontal scale bar indicates the real scale of the images. Different zones in cement (Cx) and in OPA (Ox) are numbered and indicated by solid lines (dotted across aggregates); the cement/claystone interface is traced with a dotted line.

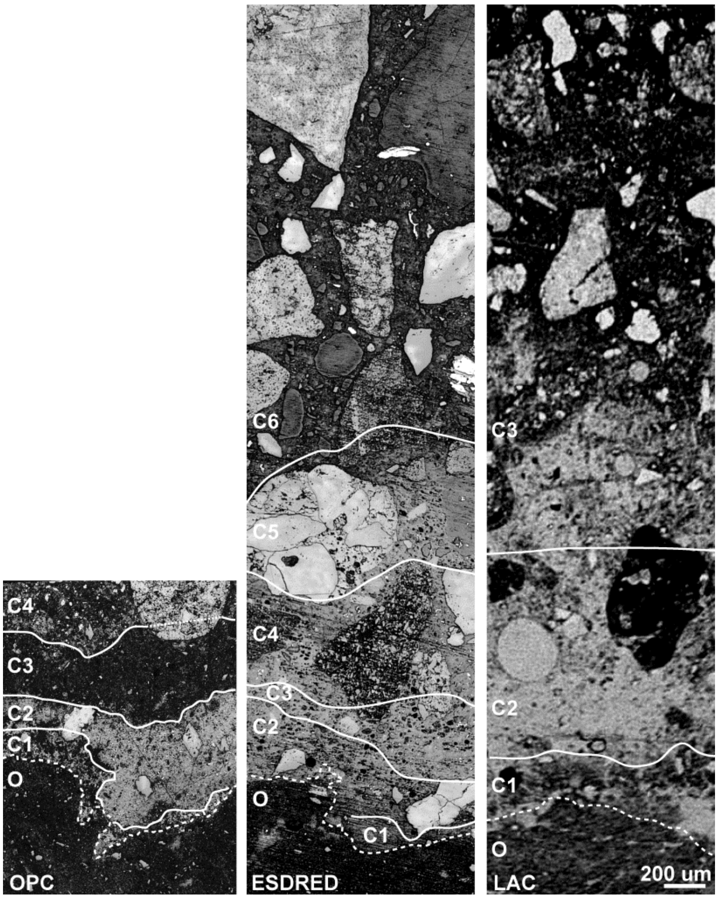

Fig. 4 Reflective light microscopic images of thin sections across the interfaces of OPC, ESDRED, and LAC at identical magnification. The interface (dotted line) divides the image into OPA (O, at the base) and cement with different interaction zones (Cx) in the same way as in Fig. 3. The light grey zones typically contain elevated carbonate content.

4.1.1. Zonation within OPC

The zone closest to the clay (C1) shows relatively high Ca in its homogeneous matrix, and it is carbonated (Fig. 4). In C1-C3, unhydrated ferrite is abundant, whereas mostly alite (Ca_3SiO_5) has transformed in-situ into a Mg-bearing hydrate. Its Mg/Al ratio is near 2 suggesting the presence of Al-hydrotalcite $Mg_4Al_2O_7(H_2O)_{10}$; the high Si and Ca content are explained by intergrowth with CSH. The Ca content in the C2 matrix is significantly lower, although this zone is still carbonated. C3 shows no more carbonation, but an increase in S and Ca within the matrix. Ca-rich patches occur, presumably portlandite. The presence of preserved clinker grains is a striking feature in C4, combined with a gradual increase in S further away from the interface. Some domains enriched in Al indicate the presence of ettringite or monosulfate phases. The S content reaches a maximum in C5 and decreases further away from the interface (C6), combined with an increased hydration of the clinker grains. The matrices of both C5 and C6 contain patches enriched in Al or Mg, and appear brighter in the BE images due to a relatively small fraction of porosity. The cement resembles undisturbed OPC at the far end.

In order to confirm the S enrichment in OPC close to claystone, aqueous leaching followed by S measurements on the residual solid were performed (Fig. 5). Bulk S measurements at different distances from the interface confirm the presence of a S-rich layer <4 mm in OPC at the interface with OPA. Neither the S map in Fig. 3, nor total or leached S show a S depletion in the cement adjacent to the enrichment. This implies that the additional S originates from OPA, and is not only a local redistributed in the cement.

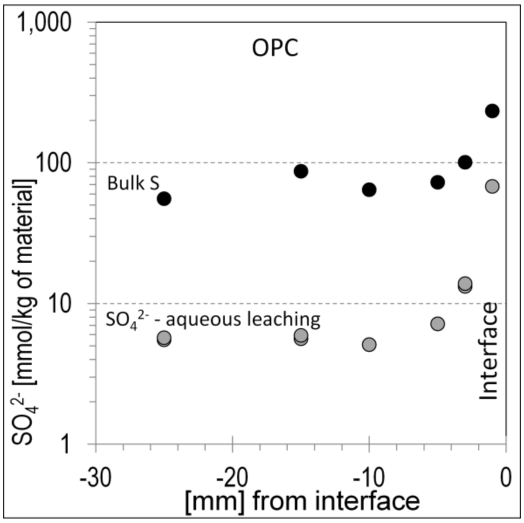

Fig. 5 SO_4^{2-} measured in leachate (liquid/solid=10 g/g), and bulk sulphur measured in OPC concrete.

4.1.2. Zonation within ESDRED

Compared to OPC, the ESDRED cement matrix contains up to twice the proportion of Si in all zones due to the addition of silica fume. In a similar way to OPC, C1 and C2 contain unhydrated ferrite skeletons with a Mg-hydrate replacing alite and belite (Ca_2SiO_4). The Mg/Al ratio of Mg-hydrate is between 1.2 and 3.2, and Si and Ca are present in excess. The matrices of C1 and C2 appear heterogeneous at the µm scale, and the individual grains are too small for EDX characterisation. In general, the thin C1 zone shows low Ca, which is higher in C2 and significantly enriched in C3. The eye-catching dark spots visible in C2 (BE image) represent Hadley grains (hollow hydration shells filled with resin during preparation). The most striking feature of C3 is its high Ca content. Almost all ferrite and in-situ Mg-hydrate have disappeared. In contrast, the C4 matrix shows lowest Ca and S and highest Mg of the entire cement contact. Ferrite and the in-situ Mg-hydrate are again present. Carbonation occurred in C1-C5 (Fig. 4). C5 appears heterogeneous: patches of portlandite, zones extremely high in Si, Mg-hydrates, and some remaining ferrite or aluminate are present. Zone C6 shows less portlandite and Mg-hydrate than C5 and resembles the undisturbed cement. C6 and the reference cement contain weakly reacted striated belite grains, which are absent in other zones.

4.1.3. Zonation within LAC

In a similar way to ESDRED, the LAC cement contains nanosilica and slag as an additional Si and Mg source compared with an OPC. Adjacent to the clay, a 200-400 µm thick layer of the LAC (C1) is significantly enriched in Mg and extensively cracked. Its homogeneous matrix has a Mg/Al ratio of ~1.9, is high in Si, but Ca is almost absent. The isolated C1 zones within C2 are expected to connect with a continuous C1 layer below or above the mapping plane. C2 consists of a hydrate matrix with a Mg content similar to the slag, and remaining slag particles with a hydration rim. C3 again shows slag particles in a hydrate matrix, which shows higher S and higher Ca than in C2. The entire LAC area shown in Fig. 3 is carbonated; the carbonation ends approximately at the upper image border (Fig. 4). XRF data (not shown) indicate an increase of S further away from the interface. Due to limited sample size, the full extent of the interaction zone might not have been captured.

4.1.4. Zonation within OPA

SEM EDX mapping reveals a 250 µm Ca-enriched layer in OPA adjacent to the OPC (O1). In addition to the elevated Ca in the homogenous clay matrix, high Ca concentrations occur in veins connected to the cement. Weak Mg and S enrichments are also suggested by numerous EDX spot measurements close to the interface. Elevated calcite content within the first mm adjacent to the interface (18 wt%, contrasting 10 wt% within 2-15 mm from contact, measured by IR spectroscopy of micro-drilled powder) confirms Ca enrichment at the interface.

The site occupancies of exchangeable cations were deduced from CEC measurements of OPA at different distances from the interface with OPC and were compared with OPA reference in order to identify changes in the cation proportions on the clay exchanger (Fig. 6). The site occupancies of exchangeable cations in OPA near the interface with OPC significantly differ from the OPA reference. Ca occupancy may be considered as constant at constant pH, because the Ca content in the pore water is controlled by Ca-carbonates (Bradbury and Baeyens, 1998). Increased pH close to OPA would decrease solubility, Ca concentration in the pore water, and Ca occupancy, which is not observed. Na and K occupancies increase at the expense of Mg towards the contact. This suggests Mg diffusion from OPA into OPC, leading to the observed precipitation of Mg hydrates. The slight CEC decrease towards the cement contact might be explained by an increasing fraction of calcite (mentioned above) or other precipitates at the expense of clay phases.

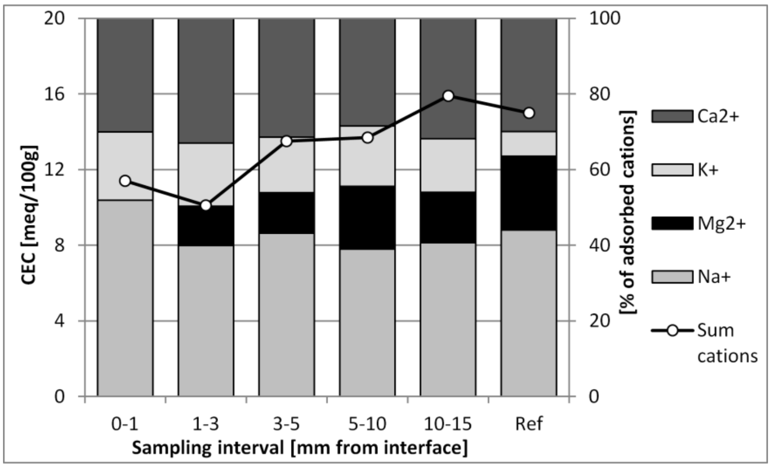

Fig. 6 Cation exchange population and CEC measured in OPA clay in contact with OPC. The reference OPA sample (Ref) was collected from borehole HT-1 (Lerouge et al., 2010), preserved in liquid nitrogen and analysed with the same procedure (cobalt hexamine trichloride, liquid/solid = 20 g/g, 30 min).

Aqueous leaching was also performed on OPA at different distances from the OPC interface and compared with well-preserved OPA sulphate reference of 2.6 mmol/kg (Lerouge et al., 2010). All concentrations of dissolved sulphate from aqueous leaching are systematically slightly higher, with a small increase at the interface, but with constant bulk sulphur content (Fig. 7). This strongly suggests a partial degradation of sulphides present in OPA (pyrite) into sulphates by oxidation. Raman spectroscopic measurements within 2 cm from all three concrete interfaces show a hematite coating on pyrite surfaces, whereas in the undisturbed OPA, pure pyrite only was identified. Neither SEM EDX nor leaching revealed a zone in OPA depleted in S that compensated the additional S found in the cement. Pyrite oxidation might have supplied the additional sulphate that was migrating into the cement without depleting the OPA pore water.

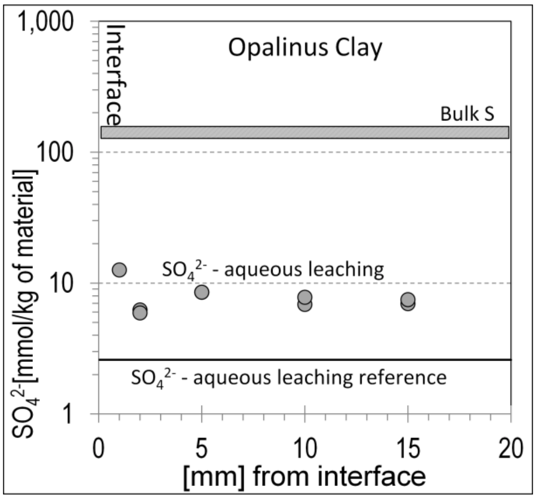

Fig. 7 SO_4^{2-} measured in leachate (liquid/solid=10 g/g) of OPA in contact with OPC, and in reference OPA (dashed line) as well as reference bulk S (grey bar). The reference OPA sample was collected from the borehole HT-1 (Lerouge et al., 2010), preserved in liquid nitrogen and analysed with the same procedure.

SEM BE images and EDX maps reveal a 250 µm Mg-enriched layer (by a factor of ~2.3) in OPA close to LAC concrete. Further weak chemical gradients in OPA are below the sensitivity of the EDX mapping, but can be shown by numerous EDX spot measurements close to the interface: Mg is also enriched in the OPA close to ESDRED, but within a thinner layer than in case of OPA-LAC, and only by a factor of ~1.3. S is also weakly enriched in a thin layer adjacent to both LAC and ESDRED cements.

At first, the chemical gradients of Ca, Mg, and S between cement and OPA pore waters (Table 1) suggest diffusion from OPA into the cements, and therefore depletion in the OPA close to the interface, contradicting the observations described above. Several considerations might explain this apparent inconsistency:

- An expected increase in pH within the OPA close to cement changes phase stabilities and therefore also pore water composition. This might locally inverse some of the overall concentration gradients shown in Table 1.
- The OPA layer influenced by ion diffusion is estimated to be ~20 cm (from Fick's second law, one dimensional, constant D_{eff}=6x10^{-11} m^2/s, constant cement pore water concentration). This is beyond the sample size available for this study. Possibly, the entire OPA analysed here was slightly depleted in Mg and S.
- Heterogeneity of OPA might mask the depletions expected to be in the range of EDX sensitivity.

Alternatively, bulk methods of material sampled from layers parallel to the interface may be more suitable to reveal larger-scale chemical heterogeneity than the localised maps.

4.2. Mineralogical interpretation of the zonation

4.2.1. Zones in cement

It is a challenge to obtain any mineralogical information on the small cement matrix volumes in between the aggregate and sand grains, and contained in the narrow interaction zones described in section 4.1. Plotting SEM EDX spot measurements on element ratio plots can be indicative if the minerals are present (Taylor and Newbury, 1984). Each measurement represents a phase assemblage because grain sizes of cement hydrates are smaller than the measured cement volume (~1 µm^3). Fig. 8 shows measurements from all three cements, grouped according to their position in the chemical zones. Compositions of expected cement hydrates are also indicated. Compositional trend lines connecting CSH and/ or portlandite with other hydrates are shown, because the former are extensively present in cement, and therefore are also expected to influence most of the spot measurements. The composition of CSH is taken from reference samples (Lothenbach, 2010); OPC: Ca/Si=1.8, Al/Ca=0.02; ESDRED: Ca/Si=1.3, Al/Ca=0.08;

LAC: Ca/Si=1.2, Al/Ca=0.12). The bulk chemical composition of the concretes is plotted for reference as a large grey dot.

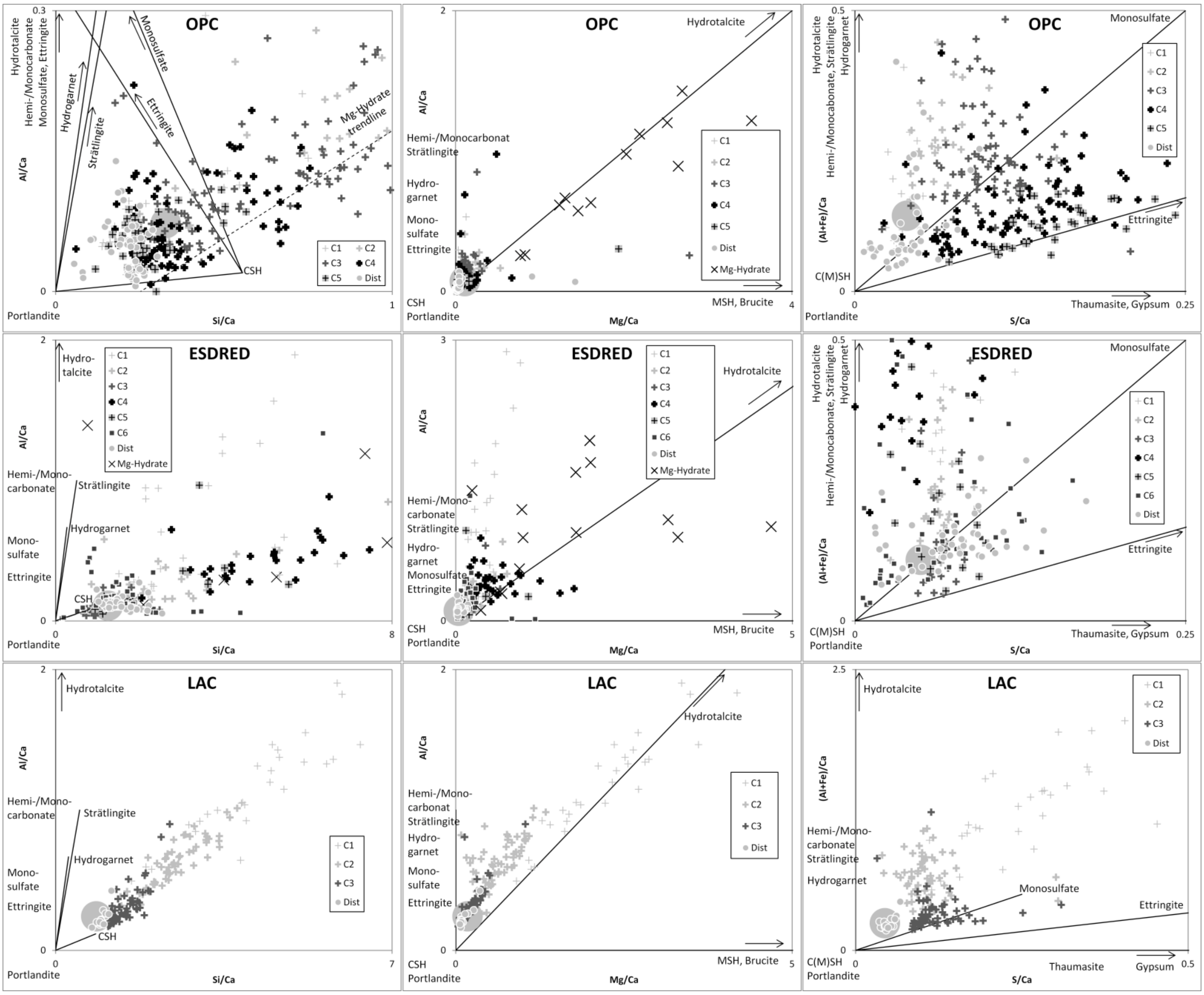

Fig. 8 Element ratio plots of SEM EDX spot measurements in OPC, ESDRED, and LAC cement matrices. Mg-hydrate measurements were performed on single grains described in sections 4.1.1 and 4.1.2. The measurements are grouped according to their position in interaction zones described in section 4.1. “Dist” denotes measurements far away from the interface in the undisturbed cement. The large grey circles correspond to the bulk chemical composition of the cement (including slag and silica). In the Si/Ca vs. Al/Ca OPC graph, the Mg-hydrates plot on a trend line (R^2=0.92) outside of the graph area (Si/Ca=2-6, Al/Ca=0.25-1.5). In the Si/Ca vs. Al/Ca ESDRED graph, most of the Mg-hydrates scatter outside of the graph area (Si/Ca=0-30, Al/Ca=0-2).

Plotting the OPC data in the diagnostic Si/Ca vs. Al/Ca diagram shows that portlandite and CSH are the main hydrates present in all interaction zones. The presence of a distinct Al-phase is unclear: Al may be incorporated in CSH. A surprising number of measurements plot to the right of the reference CSH (higher Si/Ca). This can be explained by the presence of CSH higher in Si, or MSH, or any other Si-phase. Measurements on the distinct Mg-hydrate grains described above plot even further to the right on a line connected to portlandite/CSH. The same measurements plot on CSH/portlandite-hydrotalcite or below (Mg/Ca vs. Al/Ca diagram), indicating the presence of hydrotalcite and MSH/brucite. Studies on MSH (Brew and Glasser, 2005) report the coexistence of CSH, MSH, brucite, and possibly hydrotalcite. The (Al+Fe)/Ca vs. S/Ca diagram for OPC indicates the presence of an Al-phase low in S in C1 and C2 (dots far away from CSH and left of CSH-monosulfate line). Data from C3 tend to be higher in monosulfate, whereas those in C4 can be interpreted as CSH/portlandite-monosulfate-ettringite assemblage. In C5, which is highest in S, ettringite seems to be the main S-phase. The measurements in undisturbed cement matrix plot close to the bulk chemistry. Few data plot below CSH-ettringite, which indicates the absence of gypsum or thaumasite. In contrast, spot measurements within zones high in S show the presence of gypsum disseminated in OPC. This area might be interpreted as weakly hydrated, where clinkers and other phases of the binder are better preserved.

The addition of fine-grained silica and slag enriched in Si relative to the cement in ESDRED and LAC increases the Si fraction in all measurements. Furthermore, literature (Taylor, 1997) reports a low portlandite content (in mature slag cements) or even its absence (mature microsilica cements), which is indicated in our data by the absence of measurements to the left of CSH - portlandite in the Si/Ca vs. Al/Ca diagram.

Data from the ESDRED cement plotted in the Si/Ca vs. Al/Ca, and Mg/Ca vs. Al/Ca diagrams do not indicate obvious phase assemblages, and rarely plot into well-defined regions. Measurements on Mg-hydrate grains scatter also, but Si/Ca and Al/Ca ratios are higher than in the remaining matrix, indicating the presence of several intergrown low-Ca phases. The S/Ca vs. Al/Ca diagram indicates some trends: data from C1, C2, and especially C4, all low in S, plot close to the CSH/ portlandite-hydrotalcite/ carbonate/ strätlingite/ hydrogarnet region, whereas C3, C5, and C6 plot within CSH/ portlandite-monosulfate-ettringite.

Data from each LAC interaction zone plot in well-defined regions in all three graphs. The further away from the interface, the closer the data plots to the reference and undisturbed cement composition. The C1 measurements (high in Mg) plot on CSH/ portlandite-hydrotalcite in the Mg/Ca vs. Al/Ca diagram, and the Si/Ca vs. Al/Ca diagram indicates the presence of additional Si-rich phases. Measurements to the right of monosulfate in the S/Ca vs. Al/Ca diagram suggest the presence of ettringite in C1. In the same system, most of C2 and C3 data plot above CSH/ portlandite-monosulfate, indicating the presence of monosulfate rather than ettringite.

The presence of significant amounts of Mg and S, compared to ordinary Portland cement, expands the number of phases to be considered. Therefore, a reduction to two compositional dimensions (ratio diagrams considering 3 components) is more non-unique and more commonly subject to an uncertain interpretation. A new statistical approach to process such multi-component data more rigorously is in progress.

Carbonation of mainly portlandite in cement leads to Ca carbonate formation, clearly visible in light microscopy (St John et al., 1998). However, such micrographs have to be interpreted with care (Fig. 4): the bright matrix present in C2 of OPC contains calcite, whereas similarly bright areas in LAC are low in calcite, based on micro-Raman measurements. All cements show a high fluorescence in Raman mode, which might cover the calcite bands in some measurements. ESDRED contains calcite in all interaction zones, being highest in C2 and almost absent in C3. Literature (Taylor, 1997) cites numerous studies that report very low portlandite contents in slag cements and microsilica cements, also confirmed by analysis of ESDRED and LAC reference samples (Lothenbach et al., 2012; Lothenbach et al., 2014), and therefore, little carbonation of portlandite is possible. Instead, CSH and aluminate hydrates transform to carbonate, resulting in calcite as the only carbonate, $SiO_2 \cdot nH_2O$, hydrated alumina (gibbsite), and remaining CSH has lower Ca/Si, as found in other studies (St John et al., 1998). However, the observed optical appearance that is similar to calcite, also in polarised light, implies the presence of another carbonate in LAC not identified by micro-Raman analysis.

The layer C1, adjacent to OPA, is lower in carbonate than C2 in all three cements. The thickness of the carbonated layer varies with the different water contents of the cements from 200-400 µm in the OPC with a water/binder weight ratio (w/b) of 0.35, 1.5-2 mm in ESDRED (w/b=0.5), to 2 mm in LAC (w/b=1.08). It seems likely that the thickness of the total interaction zone correlates with permeability, and hence capillary porosity, and therefore with w/b.

4.2.2.Zones in OPA

The thin and irregular interaction layers observed in Fig. 3 could not be analysed separately. IR spectroscopy of samples from three layers (0-1 mm, 3-5 mm, 10-15 mm from OPC interface) resulted in identical bands that are related to the clay fraction. This indicates a relatively homogeneous clay mineralogy near the interface.

Calcitic bioclasts and quartz grains occur in the entire OPA; small-scale heterogeneities originate from sedimentary textures. Similar conclusions are drawn from a qualitative SEM investigation of pyrite grains in OPA between 0 and 16 mm away from concrete: the different grain sizes, morphologies, and associations observed were not related to the distance from concrete. However, Raman measurements reveal surface oxidation on pyrite within 2 cm adjacent to concretes.

Narrow calcite veins extend from the OPC interface ~50 µm into OPA (observed by SEM EDX and identified by Raman). This might cause the elevated calcite content measured by IR spectroscopy within the first mm adjacent to the interface (18 wt%, contrasting with 10 wt% within 2-15 mm from the interface).

4.3. Influence of phase transformations on porosity (OPC-OPA)

If ion diffusion in the pore water across the interface led to precipitation and clogging of the entire pore space, and the new phase assemblage was at equilibrium, then interaction would stop (Marty et al., 2009). Therefore, investigation of porosity distribution perpendicular to the interface is essential in order to understand the evolution of geochemical interaction with time, a key to attempt meaningful forward predictions. In general, carbonation as discussed above causes pore space clogging (Gaboreau et al., 2012; Glasser and Matschei, 2007), well-known from concrete surfaces exposed to wet conditions and atmospheric CO_2.

Porosimetry analysis of the OPC-OPA interface resulted in the autoradiograph shown in Fig. 9 and derived total porosity values of select homogeneous matrix areas (Table 4). Segmentation of the autoradiograph data allows exclusion of aggregates, sand grains, and OPA (Fig. 10). The remaining cement matrix shows an obvious zone of lower porosity parallel to the interface, but not directly adjacent to it. The thickness of this zone is approximately 1.2 mm, and it is of the same order of magnitude as the thickness of carbonation shown in Fig. 4 (~0.5 mm). Quantification of porosities within this zone (M1, M2) reveal values near 20%, whereas areas further away from the interface show values larger than 27% (Table 4). The large scatter of the latter is attributed to porosity inhomogeneities associated with aggregate boundaries. Furthermore, a much lower porosity around 10% is expected in aged undisturbed Portland cement paste with w/c=0.35. The presence of weakly hydrated clinker especially in C4 (described above) indicates a low degree of hydration, compatible with the observed rather high porosity. In contrast, total porosities in homogeneous OPA show constant values around 21%, which agrees with reference values (Pearson et al., 2003).

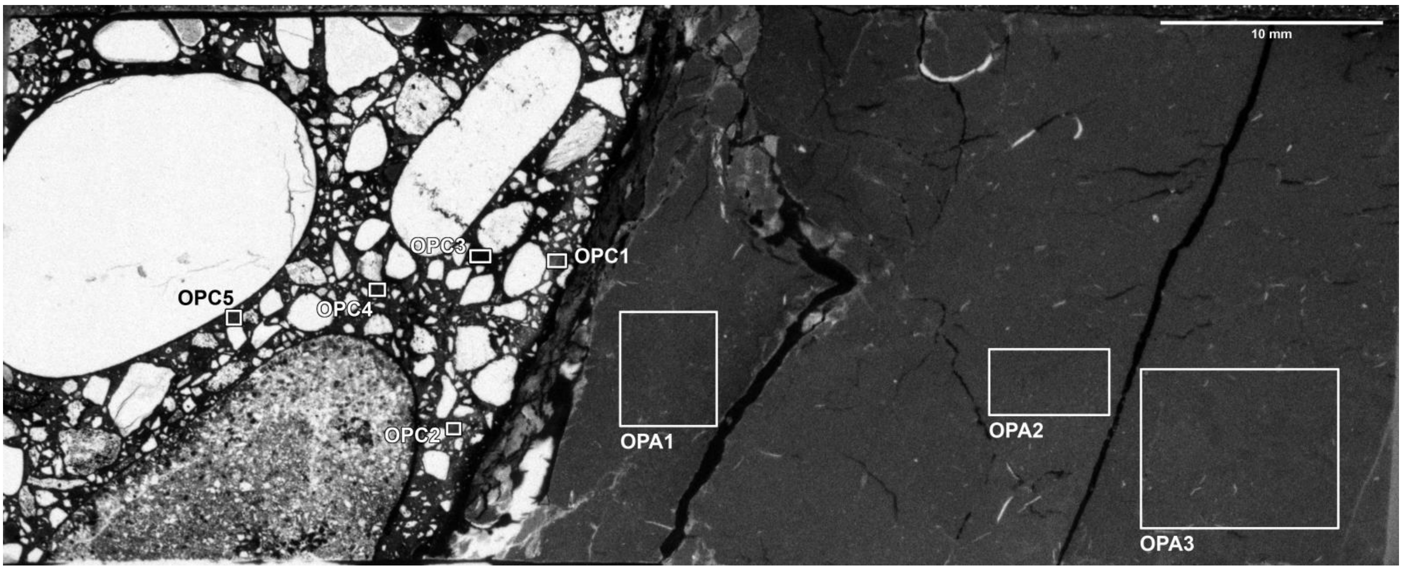

Fig. 9 Autoradiograph of the OPC (left)-OPA (right) interface. Dark areas represent high total porosity, bright areas low total porosity. Labelled squares represent quantified areas.

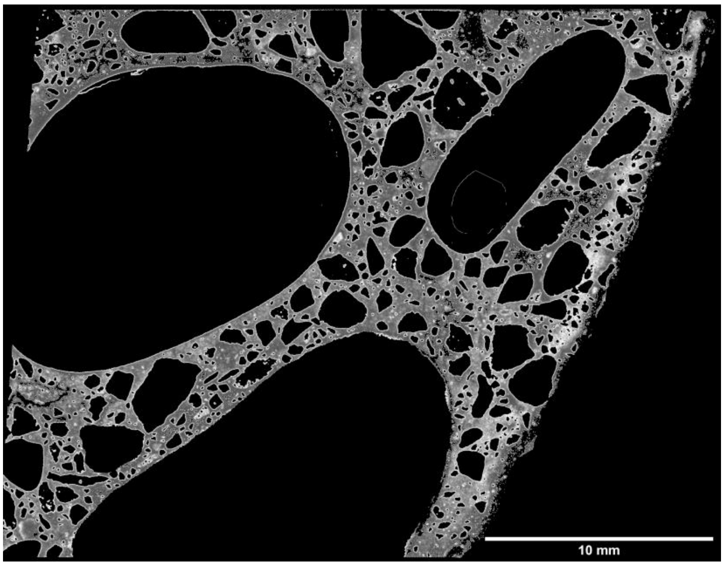

Fig. 10 Processed concrete side of the autoradiograph in Fig. 9. Aggregates, sand grains, and OPA are black, contrast and brightness of remaining cement matrix is enhanced. Dark grey areas represent high total porosity, bright areas low total porosity.

OPC matrix

area	total porosity (%)
1	18.5
2	21.9
3	53.6
4	32.2
5	27.2

OPA matrix

area	total porosity (%)
1	22.4
2	20.6
3	20.5

Table 4 Quantification of total porosity in areas labelled in Fig. 9.

5. Conclusions: interpretation of mechanisms

The diverse chemical information combined with limited mineralogical data from the different zones of interaction allow for the interpretation of possible mechanisms that caused alteration of cements and OPA over the course of 2.2 years. All mechanisms are related to ion diffusion caused by the chemical gradients between OPA and cement pore water (Table 1) that also will evolve with time. Several unknown parameters complicate the estimation of net ion diffusions based on theoretical considerations. Controlling parameters are:

- diffusion coefficients in water (known)
- ion concentration gradients (known at start, different for each cement)
- time interval during which diffusion was active (unknown, different for each cement)
- spatial evolution of capillary porosity (porosity known from w/b at start, limited data from autoradiographs at sampling interval, porosity evolution of undisturbed cements known from reference samples, different for each cement)

The presence of unhydrated clinker grains and gypsum in C4-C6 of OPC, as well as the unusual high porosity, suggests a water deficiency in this concrete with such a low w/b=0.35. Despite many efforts, the OPA borehole walls are expected to dry slightly before concrete casting. As soon as the concrete is in place, water might be sucked into the dry OPA and hinder cement hydration. With time, water pressure equilibrates again, and water chemically equilibrated with OPA moves back into dry cement, leading to a secondary hydration and conversion of alite into the unusual in-situ Mg-hydrate. Carbonation would slow down this secondary hydration by porosity reduction and a zone of unhydrated clinker may remain. However, this mechanism is considered a special case caused by the atypically low water content of this OPC (sealing plug).

5.1. Carbonation

Carbonate species, mainly bicarbonate and Ca-bicarbonate, diffuse from OPA into cement and react with the calcium hydrates. In the case of OPC, mainly calcite is formed with a net volume increase leading to pore space clogging. Calcite formation competes with portlandite dissolution caused by the penetration of low pH conditions from OPA and subsequent decalcification, as described elsewhere (Dauzères et al., 2010). The C2 layer in OPC, lowest in Ca, represents a relict of this mechanism. The temporarily high Ca concentration in the cement pore water causes Ca diffusion into OPA, leading to the observed layer enriched in Ca and the small calcite veins. No obvious mechanism was found so far explaining the elevated Ca and lower extent of carbonation in C1.

In general, the higher w/b in ESDRED and LAC results in higher capillary porosity and permeability that enables the carbonate species to diffuse deeper into the cement. Although other parameters mentioned above may have an influence, the thickness of the carbonation layer appears to depend strongly on the initial w/b. The nature of the carbonate in LAC is still unclear.

5.2. Sulphur migration and related cement hydrates

While it is known that sulphur in OPA pore water is largely sulphate rather than sulphide, this is also known for OPC, but especially LAC may contain some minor proportion of reduced sulphur species, such as thiosulphate (Lothenbach et al., 2012). Here, we focus on the dominant sulphur components and implicitly assume that S occurs mostly as sulphate. Approximately 1 day after mixing, S concentration in OPC pore water drops below the concentration in OPA (Lothenbach and Winnefeld, 2006). From then onwards, S species diffuse into OPC. Due to the lowering of pH in cement (OPA interaction and carbonation), no sulphate-bearing hydrates can form. S diffuses deeper into the cement, until pH conditions high enough for precipitation of monosulfate and ettringite are encountered. Element ratio plots indicate the presence of monosulfate in C3/ C4 and ettringite in C4/ C5, consistent with the fact that monosulfate can form at lower S concentrations than ettringite. Finally, the C5 layer forms that is most enriched in S.

Although a similar evolution of S concentration may be expected in ESDRED, the S enrichment is much less pronounced than in OPC. The thicker carbonation layer might have lowered pH in the already low-pH environment of ESDRED more than in OPC, and this might have hindered diffusion at an earlier stage due to pore clogging.

The slag component in LAC releases reduced S species in addition to the sulphates commonly contained in cements. This may lead to higher S concentration in the pore solution also in older LAC, to a lower gradient between LAC and OPA pore water, and therefore to a lower S uptake from OPA. Zone C3 is slightly enriched in S, attributed to the formation of monosulfate. Whereas the S enrichments in LAC and ESDRED might originate from S redistribution within the cement itself, the strong enrichment in the OPC can only be caused by additional S coming from the OPA.

5.3. Magnesium migration

The gradient in Mg between cement and OPA pore water is ~4 orders of magnitude. Therefore, Mg migrates into the cement. In OPC and ESDRED, the Mg reacts with alite forming an in-situ Mg-hydrate, presumably hydrotalcite. More distant from the OPA in ESDRED (C4), chemical conditions favour precipitation of Mg-hydrate not restricted to alite grains; the associated element ratio plot indicates the presence of MSH rather than hydrotalcite.

The substantial Mg uptake in the LAC layer closest to OPA leads to formation of presumably MSH intergrown with other hydrates. The cracking observed in this layer is known from the formation of MSH (Dauzères, 2010).

The cations populating the clay mineral's exchange sites serve as readily available Mg reserve for the OPA pore water: within a 1 mm thick OPA layer adjacent to OPC, Mg disappears from the exchange sites of the clay minerals and is compensated by Na. A much thinner OPA layer (0.2 mm) at the interface enriched in Mg cannot be explained at present, but it is assumed to have formed during a different time interval than the Mg migration from OPA into cement.

5.4. Precipitation in OPA

The present study did not reveal any zone of reduced porosity within OPA next to OPC. The calcite enrichment adjacent to the contact observed by IR spectroscopy can be explained by calcite veins extending from OPC into the OPA, presumably filling up small cracks caused by drilling into the OPA before casting of concrete.

Literature (Dauzères, 2010; Dauzères et al., 2010) states smectite-illite transformation due to K migration from cement into clay stone based on XRD analyses. The diffractogram interpretation carried out is disputable, because ion exchange on smectite and water content can result in similar pattern modification (Ferrage et al., 2011; Morodome and Kawamura, 2009). Regarding chemistry, the net increase in K of the OPA for smectite-illite transformation is below 1 mol% (total smectite content in OPA is around 5 wt%, occurring as illite-smectite mixed layers) and therefore close to or below the sensitivity of SEM EDX. However, IR spectroscopy revealed no changes in clay mineralogy at different distances from the contact. The available sample geometry and volume did not permit more appropriate analysis like bulk XRD, and this issue cannot be addressed in the present study.

6. Outlook

Thermodynamic equilibrium between cement and clay stone is achieved at complete homogenisation. The formation of a low porosity layer at the interface within concrete or clay stone can delay and eventually inhibit this progress. But the system will evolve towards local equilibrium on both sides with the phases clogging the pore space. Possibly, carbonation may lead to such a state. The estimated porosity in OPC at the interface after 2.2 years of OPA interaction is 20% and carbonate filled up at least 7%. The investigation of older samples, also with higher initial w/c ratio, where normal cement hydration is expected (presently on-going) will show if carbonation is further reducing porosity. The mechanisms mentioned above cannot be considered independently, however, because they strongly influence each other. Therefore, numerical modelling is planned in order to increase the understanding of the entire clay stone-cement interaction, of which the results of this study only represent one snapshot of the consequences.

Slow kinetics might also prevent complete homogenisation within a time interval of interest. With respect to clay phase stability, it is unclear if reactions are too slow to result in measurable changes, or if no reaction at all occurs. This fundamental difference is of importance with respect to forward predictions; again, examination of older samples in years to come might answer this question.

Furthermore, micro-XRD techniques are being developed in order to measure sample volumes small enough to probe a single interaction layer between the aggregate. The resulting spatially resolved phase identity will further constrain the mechanisms mentioned above or expose new ones.

The interaction experiment continues without any maintenance or monitoring, if lateral sampling boreholes are properly sealed as done after the 2.2 and 5 years sampling campaign. Therefore, the foreseen experiment duration of 20 years, including further sampling, is realistic.

Acknowledgements

Most of the analytical results presented here rely on samples carefully crafted by the rock preparation team of the Institute of Geological Sciences, University of Bern (Stephan Brechbühl, Thomas Aebi). The CI Project is funded by ANDRA, CRIEPI, IRSN, Nagra, Obayashi, and SCK•CEN. The scientific and technical team operating the Mont Terri facility (Swisstopo) is acknowledged for field support. Drilling was kindly performed by Hans Abplanalp (Nagra).

References

Adler, M., 2001. Interaction of claystone and hyperalkaline solutions at 30 °C: A combined experimental and modeling study. University of Bern, Switzerland, Bern.

Adler, M., Mäder, U., Waber, H.N., 2001. Core infiltration experiment investigating high-pH alteration of low-permeability argillaceous rock at 30 ºC, in: Cidu, R. (Ed.), Proceedings WRI-10 (10th International Symposium on Water-Rock Interaction). Balkema, Villasimius, Italy, pp. 1299-1302.

ANDRA, 2005. Dossier 2005 argile synthesis: Evaluation of the feasibility of a geological repository in an argillaceous for mation. Meuse/haute-marne site, in: ANDRA Report Series, ANDRA.

Bradbury, M.H., Baeyens, B., 1998. A physicochemical characterisation and geochemical modelling approach for determining porewater chemistries in argillaceous rocks. Geochim. Cosmochim. Acta 62, 783-795.

Brew, D.M.R., Glasser, F.P., 2005. The magnesia-silica gel phase in slag cements: Alkali (K, Cs) sorption potential of synthetic gels. Cem. Concr. Res. 35, 77-83.

Ciesielski, H., Sterckeman, T., 1997. A comparison between three methods for the determination of cation exchange capacity and exchangeable cations in soils. Agronomie 17, 9-16.

Dähn, R., Popov, D., Schaub, P., Pattison, P., Grolimund, D., Mäder, U., Jenni, A., Wieland, E., 2014. In-situ x-ray micro-diffraction studies of heterogeneous interfaces between cementitious materials and geological formations. Phys. Chem. Earth (this issue).

Dauzères, A., 2010. Etude expérimentale et modélisation des mécanismes physico-chimiques des interactions béton-argile dans le contexte du stockage géologique des déchets radioactifs, Laboratoire d'Hydrogéologie Argiles Sols et Altérations. Université de Poitiers, Poitiers, p. 272.

Dauzères, A., Le Bescop, P., Sardini, P., Coumes, C.C.D., 2010. Physico-chemical investigation of clayey/cement-based materials interaction in the context of geological waste disposal: Experimental approach and results. Cem. Concr. Res. 40, 1327-1340.

De Windt, L., Marsal, F., Tinseau, E., Pellegrini, D., 2008. Reactive transport modeling of geochemical interactions at a concrete/argillite interface, Tournemire site (France). Phys. Chem. Earth 33, S295-S305.

Ferrage, E., Vidal, O., Mosser-Ruck, R., Cathelineau, M., Cuadros, J., 2011. A reinvestigation of smectite illitization in experimental hydrothermal conditions: Results from x-ray diffraction and transmission electron microscopy. Am. Mineral. 96, 207-223.

Gaboreau, S., Lerouge, C., Dewonck, S., Linard, Y., Bourbon, X., Fialips, C.I., Mazurier, A., Pret, D., Borschneck, D., Montouillout, V., Gaucher, E.C., Claret, F., 2012. In-situ interaction of cement paste and shotcrete with claystones in a deep disposal context. Am. J. Sci. 312, 314-356.

Gaboreau, S., Prêt, D., Tinseau, E., Claret, F., Pellegrini, D., Stammose, D., 2011. 15 years of in situ cement-argillite interaction from Tournemire URL: Characterisation of the multi-scale spatial heterogeneities of pore space evolution. Appl. Geochem. 26, 2159-2171.

Galle, C., 2001. Effect of drying on cement-based materials pore structure as identified by mercury intrusion porosimetry - a comparative study between oven-, vacuum-, and freeze-drying. Cem. Concr. Res. 31, 1467-1477.

Glasser, F.P., Matschei, T., 2007. Interactions between portland cement and carbon dioxide, 12th International Congress on the Chemistry of Cement, Montreal, Canada.

Hellmuth, K.H., Siitarikauppi, M., Lindberg, A., 1993. Study of porosity and migration pathways in crystalline rock by impregnation with C-14 polymethylmethacrylate. J. Contam. Hydrol. 13, 403-418.

Jenni, A., Mäder, U., Lerouge, C., Gaboreau, S., Schwyn, B., 2012. Concrete-Opalinus clay interaction, in: ANDRA (Ed.), 5th Meeting on Clays in Natural and Engineered Barrier for Radioactive Waste Confinement, Montpellier, France.

Jenni, A., Mäder, U., Lerouge, C., Gaboreau, S., Schwyn, B., 2013. Concrete-Opalinus clay interaction, 3rd International Workshop Mechanisms and Modelling of Waste/Cement Interactions, Gent, Belgium.

Kosakowski, G., Berner, U., 2013. The evolution of clay rock/cement interfaces in a cementitious repository for low- and intermediate level radioactive waste. Phys. Chem. Earth 64, 65-86.

Lerouge, C., Gailhanou-Vigier, H., Marty, N., Blanc, P., Auger, P., Flehoc, C., Gautier, A., Haas, H., Henry, B., Jean-Prost, V., Wille, G., 2010. Mineralogy and geochemistry of cores of the BHT-1 borehole, Mont Terri rock laboratory, BRGM, p. 51.

Lothenbach, B., 2010. Ci experiment: Hydration experiments of OPC, LAC and ESDRED cements: 1 h to 3.5 years, TN 2010-75, Mont Terri Project.

Lothenbach, B., Le Saout, G., Ben Haha, M., Figi, R., Wieland, E., 2012. Hydration of a low-alkali CEM III/b-SiO2 cement (LAC). Cem. Concr. Res. 42, 410-423.

Lothenbach, B., Rentsch, D., Wieland, E., 2014. Hydration of a silica fume blended low-alkali shotcrete cement. Phys. Chem. Earth (this issue).

Lothenbach, B., Wieland, E., 2006. A thermodynamic approach to the hydration of sulphate-resisting Portland cement. Waste Manage. 26, 706-719.

Lothenbach, B., Winnefeld, F., 2006. Thermodynamic modelling of the hydration of Portland cement. Cem. Concr. Res. 36, 209-226.

Marty, N.C.M., Tournassat, C., Burnol, A., Giffaut, E., Gaucher, E.C., 2009. Influence of reaction kinetics and mesh refinement on the numerical modelling of concrete/clay interactions. J. Hydrol. 364, 58-72.

Morodome, S., Kawamura, K., 2009. Swelling behavior of Na- and Ca-montmorillonite up to 150 degrees C by in situ x-ray diffraction experiments. Clays Clay Miner. 57, 150-160.

Nagra, 2002. Project Opalinus clay - safety report: Demonstration of disposal feasibility for spent fuel, vitrified high-level waste and long-lived intermediate level waste (Entsorgungsnachweis), in: Nagra Technical Report, NTB 02-05, Nagra, Wettingen, Switzerland.

Pearson, F.J., Arcos, D., Bath, A., Boisson, J.-Y., Fernández, A.M., Gäbler, H.-E., Gaucher, E., Gautschi, A., Griffault, L., Hernán, P., Waber, H.N., 2003. Mont Terri Project – geochemistry of water in the Opalinus clay formation at the Mont Terri rock laboratory, in: Berichte des BWG, Serie Geologie, 5, BWG, Bern.

Pret, D., Sammartino, S., Beaufort, D., Fialin, M., Sardini, P., Cosenza, P., Meunier, A., 2010. A new method for quantitative petrography based on image processing of chemical element maps: Part II. Semi-quantitative porosity maps superimposed on mineral maps. Am. Mineral. 95, 1389-1398.

Pret, D., Sardini, P., Beaufort, D., Zellagui, R., Sammartino, S., 2004. Porosity distribution in a clay gouge by image processing of C-14-polymethylmethacrylate (C-14-PMMA) autoradiographs: Case study of the fault of St. Julien (basin of Lodeve, France). Appl. Clay Sci. 27, 107-118.

Read, D., Glasser, F.P., Ayora, C., Guardiola, M.T., Sneyers, A., 2001. Mineralogical and microstructural changes accompanying the interaction of Boom Clay with ordinary Portland cement. Adv. Cem. Res. 13, 175-183.

Rémy, J.C., Orsini, L., 1976. Utilisation du chlorure de cobaltihexamine pour la détermination simultanée de la capacité d'échange et des bases échangeables dans les sols. Sciences du Sol 4.

Sammartino, S., Siitari-Kauppi, M., Meunier, A., Sardini, P., Bouchet, A., Tevissen, E., 2002. An imaging method for the porosity of sedimentary rocks: Adjustment of the PMMA method - example of a characterization of a calcareous shale. J. Sediment. Res. 72, 937-943.

SCK•CEN, 2012. Preparatory safety assessment. Conceptual model description of the reference case, in: External Report of the Belgian Nuclear Research Centre, ER-215, CCHO - 2009-00940000, SCK•CEN, Mol, Belgium, p. 95.

St John, D.A., Poole, A.W., Sims, I., 1998. Concrete petrography: A handbook of investigative techniques.

Taylor, H.F.W., 1997. Cement chemistry, 2 ed. Thomas Telford Publishing, London.

Taylor, H.F.W., Newbury, D.E., 1984. An electron microprobe study of a mature cement paste. Cem. Concr. Res. 14, 565-573.

Tinseau, E., Bartier, D., Hassouta, L., Devol-Brown, I., Stammose, D., 2006. Mineralogical characterization of the Tournemire argillite after in situ interaction with concretes. Waste Manage. 26, 789-800.